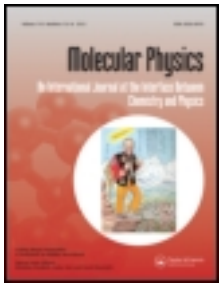

Molecular Physics: An International Journal at the Interface Between Chemistry and Physics
Publication details, including instructions for authors and subscription information:
http://www.tandfonline.com/loi/tmph20

Figuration and detection of single molecules

R. Nevels [a], G.R. Welch [a], P.S. Cremer [a], P. Hemmer [a], T. Phillips [a], S. Scully [a], A.V. Sokolov [a], A.A. Svidzinsky [a b], H. Xia [b], A. Zheltikov [a] & M.O. Scully [a b]

[a] Texas A&M University, College Station, TX 77843, USA

[b] Princeton University, Princeton, NJ 08544, USA

Accepted author version posted online: 02 Jul 2012.Version of record first published: 18 Jul 2012.

To cite this article: R. Nevels , G.R. Welch , P.S. Cremer , P. Hemmer , T. Phillips , S. Scully , A.V. Sokolov , A.A. Svidzinsky , H. Xia , A. Zheltikov & M.O. Scully (2012): Figuration and detection of single molecules, Molecular Physics: An International Journal at the Interface Between Chemistry and Physics, 110:15-16, 1993-2000

To link to this article: http://dx.doi.org/10.1080/00268976.2012.706326

Molecular Physics
Vol. 110, Nos. 15–16, 10–20 August 2012, 1993–2000

Taylor & Francis
Taylor & Francis Group

INVITED ARTICLE

Figuration and detection of single molecules†

R. Nevels[a], G.R. Welch[a], P.S. Cremer[a], P. Hemmer[a], T. Phillips[a], S. Scully[a], A.V. Sokolov[a], A.A. Svidzinsky[ab], H. Xia[b], A. Zheltikov[a] and M.O. Scully[ab]*

[a]*Texas A&M University, College Station, TX 77843, USA;* [b]*Princeton University, Princeton, NJ 08544, USA*

(*Received 20 December 2011; final version received 19 June 2012*)

Recent advances in the description of atoms and molecules based on Dimensional scaling analysis, developed by Dudley Herschbach and co-workers, provided new insights into visualization of molecular structure and chemical bonding. Prof. Herschbach is also a giant in the field of single molecule scattering. We here report on the engineering of molecular detectors. Such systems have a wide range of application from medical diagnostics to the monitoring of chemical, biological and environmental hazards. We discuss ways to identify preselected molecules, in particular, mycotoxin contaminants using coherent laser spectroscopy. Mycotoxin contaminants, e.g. aflatoxin B1 which is present in corn and peanuts, are usually analysed by time-consuming microscopic, chemical and biological assays. We present a new approach that derives from recent experiments in which molecules are prepared by one (or more) femtosecond laser(s) and probed by another set. We call this technique FAST CARS (femto second adaptive spectroscopic technique for coherent anti-Stokes Raman spectroscopy). We propose and analyse ways in which FAST CARS can be used to identify preselected molecules, e.g. aflatoxin, rapidly and economically.

Keywords: Raman spectroscopy; CARS; SERS; nanoantenna array

1. The Bohr–Herschbach picture of a molecule

'The great Dudley Herschbach' is the accolade applied to our distinguished colleague by *Newsweek Magazine*. We personally have been deeply enriched and enchanted by many things we have learned from Prof. Dudley Herschbach; not the least of which is his dimensional scaling analysis to many electron atoms and molecules [1–3]. In particular, in a PRL devoted to this technique entitled 'Simple and Surprisingly Accurate Approach to the Chemical Bond Obtained from Dimensional Scaling' [4] we, together with Dudley Herschbach, developed a description of the electronic molecular structure based on the D-scaling approach adapted from Quantum Chromodynamics by generalizing the Schrödinger equation to D-dimensions and rescaling coordinates. This approach treats electrons as point particles whose positions are determined by optimizing an algebraic energy function derived from the large-dimension limit of the Schrödinger equation. The calculations required are simple yet yield useful accuracy for molecular potential curves and bring out appealing heuristic aspects. When this procedure is applied to the simple hydrogen atom we obtain in the $D \to \infty$ limit the Bohr planetary orbit results [5,6]. Higher order corrections in $1/D$, in general, lead to an improvement in the accuracy of the D-scaling treatment.

When we apply this technique to the two-centre problem, such as the H_2 molecule, we have to re-evaluate and correct Bohr's ingenious 1913 molecular model [6]. Bohr's insightful picture of a molecule (see Figure 1) has much to recommend, but fell short of catching the public eye because binding goes wrong for large interatomic spacing. This is essentially due to the fact that of the four possible configurations [7], Bohr found only the symmetric one. In particular, Bohr says in his hand written notes [8]: 'The model proposed for H_2 seems to be the only possible equilibrium figuration of 2 kerns and 2 electrons (looking apart from two separate atoms), in which the kerns are at rest'.

Clearly the Bohr symmetric picture of the H_2 molecule goes wrong at large separation, but it has much correct physics in it. It is unfortunate that it didn't catch on earlier. Bohr in his 1913 molecular paper [6] did present the germ of the idea, but

*Corresponding author. Email: scully@tamu.edu
†It is a pleasure to dedicate this article to Prof. Dudley R. Herschbach, researcher, teacher and colleague extraordinaire. He is a role model for us all.

ISSN 0026–8976 print/ISSN 1362–3028 online

http://dx.doi.org/10.1080/00268976.2012.706326
http://www.tandfonline.com

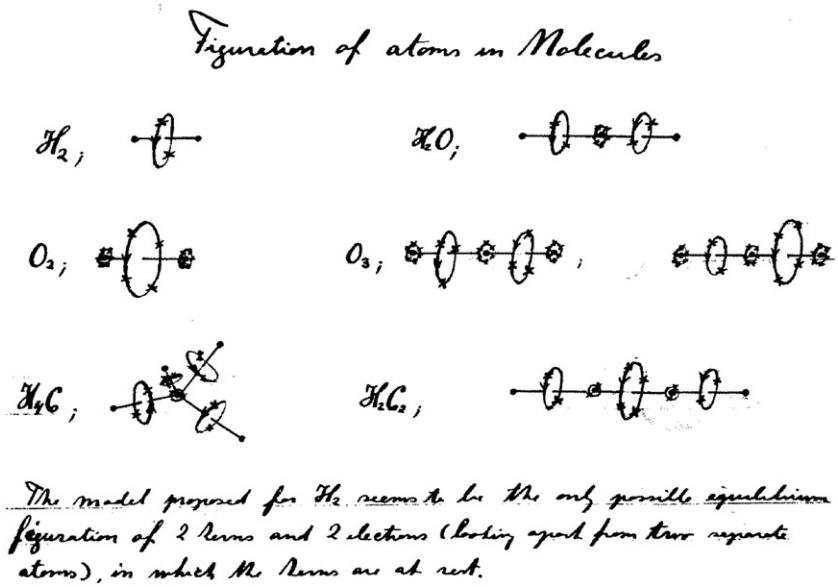

Figure 1. Molecular configurations as sketched by Niels Bohr; from an unpublished manuscript [8], intended as an appendix to his 1913 papers.

Sommerfeld in his famous book provided the following assessment [9]: 'We shall now describe a little more fully the model that Bohr has suggested for the constitution of the hydrogen molecule H_2, although nowadays we can only take a historical interest in it.' After a little discussion he asks 'but, is it correct?' and then he goes on to say: 'only a short while ago, even while this book was in its first edition, we were inclined to accept it'. However later in the book he mentions 'thus the true model of H_2 is still unknown, it will hardly be as symmetrically built as the model exhibited in Figure 1'.

Indeed we found that the asymmetric arrangement (2) shown in Figure 2 (top) constitutes the 'correct' model of H_2 [7]. This is clearly demonstrated by the potential energy curves plotted in Figure 2 for the symmetric (1) and asymmetric (2) electron configurations. The asymmetric configuration gives lower energy and yields the correct dissociation limit of H_2 at large internuclear spacing R. Dimensional scaling analysis can improve the accuracy. In fact, including the first $1/D$ correction yields a very nice result close to the 'exact' quantum mechanical answer (see dashed line in Figure 2).

In another paper, Gilbert N. Lewis comments on Bohr's ideas saying [10]:

> 'The other way in which one body may hold another is that in which the planets are held by the sun, and this is the way that in some current theories of atomic structure the electrons are supposed to be held by the atom. The most interesting and suggestive of these

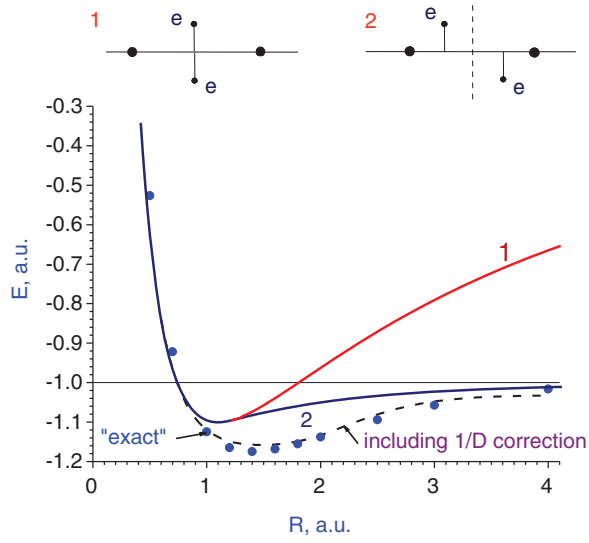

Figure 2. Energy $E(R)$ of H_2 molecule for two electron configurations (top) as a function of internuclear distance R calculated within the Bohr model (solid lines) and the 'exact' ground state energy (dots) obtained by numerical solution of the Schrödinger equation. Unit of energy is 1 au = 27.21 eV, and unit of distance is the Bohr radius. Curve 1 corresponds to Bohr's symmetric configuration of the H_2 molecule sketched in Figure 1 which yields dissociation of H_2 into separate electrons and protons at large R. Curve 2 corresponds to the asymmetric configuration and describes dissociation of H_2 into two hydrogen atoms. Dashed line is obtained using D-scaling analysis by including a $1/D$ correction [4].

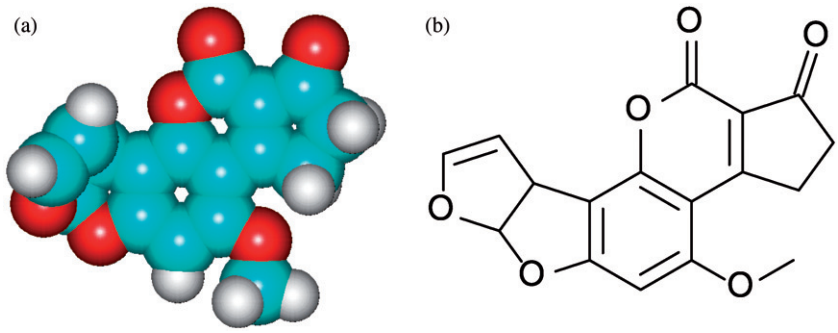

Figure 3. (a) Molecular model of aflatoxin B_1 showing the spatial orientation of functional groups. Key: light grey is hydrogen; cyan is carbon; red is oxygen. (b) Chemical structure of Aflatoxin B1 [13].

theories is the one proposed by Bohr and based upon Planck's quantum theory. Planck in his elementary oscillator which maintains its motion at the absolute zero, and Bohr in his electron moving in a fixed orbit, have invented systems containing electrons of which the motion produces no effect upon external charges. Now this is not only inconsistent with the accepted laws of electromagnetism but, I may add, is logically objectionable, for that state of motion which produces no physical effect whatsoever may better be called a state of rest.'

Dimensional scaling analysis provides connection between quantum mechanics and the Bohr model. Namely, in the limit $D \to \infty$ the Schrödinger equation reduces to finding extrema of the Bohr model algebraic energy function [4]. However, at large D electrons acquire large effective mass and, hence, for $D \to \infty$ they do not move. In the D-scaled space, they assume fixed positions relative to the nuclei and each other that correspond to the minimum of the effective potential. This is 'state of rest' mentioned by Lewis. Thus, the large-D limit belatedly reconciles the Bohr model with the more rudimentary prequantum 'static atom' description advanced in 1916–1923 by Gilbert Lewis and Irving Langmuir.

Thus, the ingenious work of Dudley Herschbach gave us insight on visualizing structure of atoms and molecules and yielded better understanding of how chemical bonds are formed [11]. Detailed knowledge of molecular properties, in particular their unique molecular vibrational signatures, is the key ingredient for their detection. Development of molecular sensors is a challenging and important task. Their application areas cover a wide range of demands from medical diagnostic to the monitoring of chemical, biological and environmental risks.

In the next sections we discuss ways how to identify preselected molecules, in particular mould toxins, rapidly and economically using coherent laser spectroscopy.

2. Engineering a laser spectroscopic detector of molecules

The rapid detection and monitoring of toxins in clinical fluids, environmental samples, food, and drinking water is important in order to expedite appropriate countermeasures. Mycotoxins (from Greek (mukos) 'fungus' and Latin (toxicum) 'poison') produced by certain fungi and moulds (e.g. aflatoxin shown in Figure 3 is produced by *Aspergillus flavus* moulds) are a major problem due to fungal infection of grains and peanuts and can still be present after food processing [12]. It is estimated that 25% of the worlds crops are contaminated to some extent. In historical context, the aflatoxin problem in foods is long-standing, unavoidable and seemingly inextricable. Aflatoxins are harmful by-products of mould growth and though invisible to the naked eye are potentially fatal to humans and animals. They are also known carcinogens.

In addition to their primary *A. flavus* origin, aflatoxins are also produced by *Aspergillus parasiticus* fungi and to a lesser extent *Aspergillus nominus*. These fungi are widespread and are especially a problem during extended periods of drought. Thus, drought stress can be a frequent harbinger of intensified production of aflatoxins in the field, a problem compounded by global warming.

Aflatoxins are heat stable and can survive a variety of food processing procedures making them 'unavoidable' contaminants in most foods (particularly those derived from maize and peanuts). Animals can also secrete carcinogenic metabolites of aflatoxin in their milk. Consequently, a variety of dairy products (including cheese and ice cream) can be contaminated with these hazardous chemicals.

It is therefore important that new techniques be developed and old ones perfected to detect trace amounts of toxins such as aflatoxin B_1 (AfB_1) and to further study the effects of binding and neutralizing their influence [14]. The latter aspect of the problem

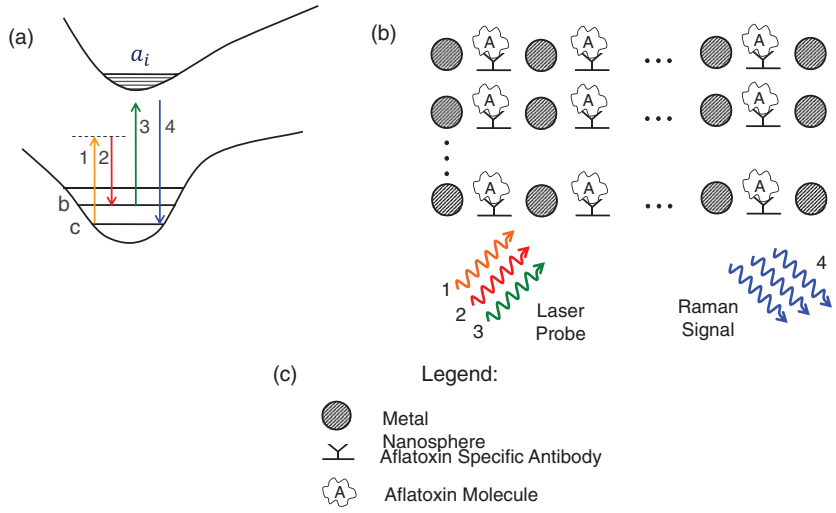

Figure 4. (a) Coherent anti-Stokes Raman scattering in which a molecule having vibrational ground state $|c\rangle$ is prepared in a coherent superposition of states $|b\rangle$ and $|c\rangle$ by pulses 1, 2. A third pulse is then scattered off the coherently oscillating molecule to produce anti-Stokes signal 4. (b) Aflatoxin molecules are bound, e.g. by antibodies sandwiched between nanospheres which are used to enhance the strength of the last field felt by the molecules. (c) Legend explaining the elements of (b).

has been addressed by the introduction of various 'detoxifying clays' into various feeds and foods.

The present scheme is summarized in Figure 4(a). The approach is based on the interplay and synergism between technologies of: Laser spectroscopy (coherent and incoherent Raman spectroscopy), Nanoscience (metal nanospheres used to create local laser field enhancement) and Toxicology (binding of AfB_1 to various smectite clays and/or to aflatoxin antigens to specific antibodies). These three parts of the detection process will be applied synergistically to optimize the detection system.

Next we review the application of coherent anti-Stokes Raman spectroscopy (CARS) for the detection of anthrax type endospores and discuss the extension of the Raman technique via nano antenna structures. Then we consider combination of these techniques to detect AfB_1 which is bound in grooves between lithographically ruled ridges.

3. Optimum pulse shape and sequence for maximizing coherent Raman signal to noise

Measurement of the vibrational spectrum of molecules by Raman spectroscopy is a common technique for species identification. In the Raman effect (see Figures 4(a) and 5(a)), lower-frequency (Stokes) radiation is emitted when laser light drives a molecule. Due to the small value of the Raman cross-section the signal is weak. However with the advent of powerful lasers, spontaneous Raman spectroscopy became a useful tool.

Moreover, when the molecules are put into coherent oscillation by a pair of preparation pulses (pulses 1 and 2 in Figure 5(b)) and a third pulse (3) is scattered by this coherent molecular vibration, a strong anti-Stokes signal (pulse 4) is generated. This process is called coherent anti-Stokes Raman scattering because the signal light is up shifted, not down shifted as in Stokes scattering (CARS). Due to the effect of coherence the CARS signal scales as the number of molecules square.

Unfortunately, CARS from the molecules of interest is frequently obscured by the non-resonant four-wave mixing (FWM) signal from other molecules (Figures 5(c) and (d)), or even from contributions from multiple off-resonant vibrational modes of the same molecules.

In recent work, we have developed techniques for maximizing the coherent molecular oscillation and minimizing the non-resonant (NR) background noise [15]. A sequence of femtosecond pulses is used so that pulses 1 and 2 prepare a coherent molecular vibration (corresponding to a particular mode of oscillation) and a third, time-delayed, probe pulse is scattered by the oscillating molecule yielding the anti-Stokes signal (Figures 5(c) and (d)). By delaying the third pulse relative to the first two, the NR FWM signal is effectively eliminated. This combination of shaped preparation pulses and an ultrashort time-delayed probe pulse maximizes the signal and reduces the background contribution (noise). We refer to this

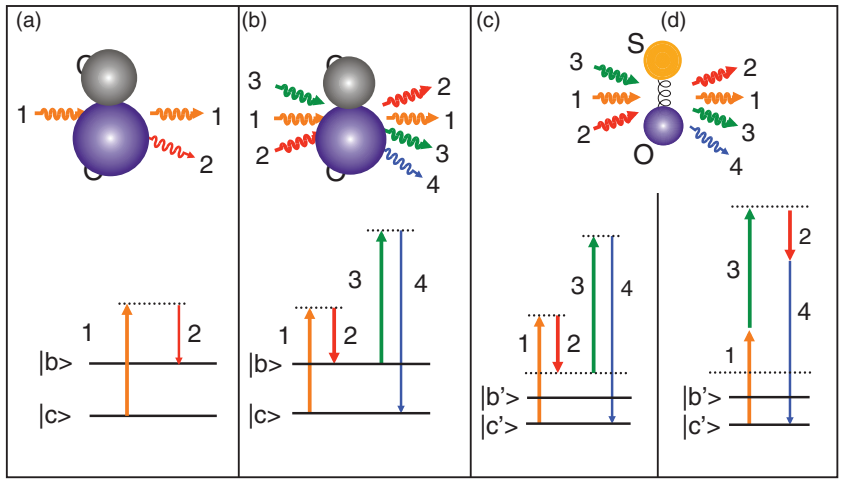

Figure 5. Level diagram and schematic of different scattering processes on simple molecules. In this example, CO is a target molecule and SO is a background molecule. Energy level c is the ground state of the CO molecule; b is the target vibrational state of the CO molecule; c' is the ground state of the background molecule; b' is an off-resonant vibrational state of the background molecule; (a) incoherent Raman scattering (pulse 2) was derived from pulse 1 scattering off the CO molecule. (b) CARS signal 4 was derived from probe pulse 3 scattering off the CO molecular vibration, coherently prepared by pulses 1 and 2. (c) One of the possible channels for the NR background generation in SO. In (d) we depict another four-wave mixing process which can contribute to the background noise.

technique as 'FAST CARS' (femtosecond adaptive spectroscopic techniques for coherent anti-Stokes Raman spectroscopy) [19]. We demonstrated utility and precision of the FAST CARS protocol in our anthrax detection experiments [16].

CARS spectroscopy/microscopy can be also improved by spectral compression of femtosecond pulses which, e.g. can be achieved by second-harmonic generation in periodically poled nonlinear crystals [17] or by use of fibre laser sources [18].

4. Application of nanostructures to enhance spontaneous Raman spectroscopy

Two decades ago it was discovered that molecules adsorbed on specially prepared silver surfaces produce a Raman spectrum that is at times a millionfold more intense than expected [20–22]. This effect was dubbed surface-enhanced Raman scattering (SERS) [23]. Colloids of silver nanoparticles [24] can enhance Raman scattering by marker molecules, and this enhancement can reach the level of detecting single molecules [25,26]. Now it is well known that SERS with metallic nanostructures [27–29] is capable of single-molecule sensitivity [30]. More recently, detailed experiments elucidate the relationship between various nanoparticles and single-molecule SERS [31,32].

To set the stage for this discussion let us begin by reviewing the basic Raman formalism and show how

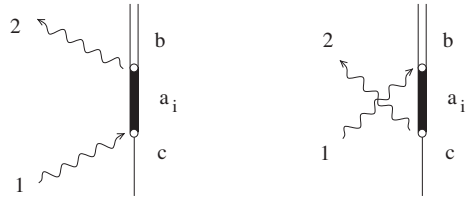

Figure 6. Time-order diagrams indicating the two contributions in Equation (1b).

the use of metal nanoparticles can enhance Raman scattering. As depicted in Figure 5(a), a molecular vibrational state is probed by a laser pulse 1 (of frequency ν_1) and a scattered photon 2 (having frequency ν_2) is observed. The Raman Hamiltonian is given by

$$H_{\mathrm{R}} = G_{b,c}|b\rangle\langle c|\hat{a}_1\hat{a}_2^{\dagger} + \mathrm{adj}, \tag{1a}$$

where $\hat{a}_2^{\dagger}$ and $\hat{a}_1$ are the creation and annihilation operators of the field modes 2 and 1, and the coupling frequency is

$$G_{ab} \simeq \sum_i \frac{\wp_{bi}\mathcal{E}_2}{\hbar}\frac{\wp_{ic}\mathcal{E}_1}{\hbar}\left[\frac{1}{\omega_i - \omega_c - \nu_1} + \frac{1}{\omega_i - \omega_b + \nu_2}\right]. \tag{1b}$$

In the preceding, the two contributions in (1b) are associated with the two time ordered diagrams indicated in Figure 6, $\wp_{bi}$ (or $\wp_{ic}$) is the matrix element

coupling the molecular states b and a_i (or a_i and c, see Figure 4(a)), $\hbar$ is Planck's constant, ε_ℓ ($\ell = 1, 2$) is the electric field per photon $(\hbar v_\ell/\varepsilon_o V)^{1/2}$ with V being the quantization volume and ε_o the vacuum permitivity, ω_m is the molecular frequency $E_m/\hbar$ where E_m is the energy of the mth level and v_ℓ is the frequency of the ℓth mode of the radiation field. One can write

$$G_{ab} \simeq \sum_i \frac{\wp_{bi}\wp_{ic}}{\epsilon_i}\varepsilon_1\varepsilon_2, \tag{2}$$

where ε_i is the energy of state $|a_i\rangle$.

When a molecule is placed between two nanoparticles the fields ε_1 and ε_2 can be enhanced by a factor α of order 10 to 1000 [33,34]. Thus in the presence of nanoparticles the effective coupling matrix element $\tilde{G}$ goes as α^2 and can be of an order 10^4 times larger for $\alpha \sim 10^2$. Furthermore, the rate of generation of signal photons goes as $\tilde{G}^2$; hence the signal photon flux is enhanced by a factor of order 10^8. It is for this reason that small scale surface roughness has been used to enhance the scattering rate of molecules on a metal surface. SERS technique has been used to detect and study single molecules, one at a time.

One should note that surface-enhanced Raman scattering can be combined with CARS which leads in enhancement in the CARS signal and improvement of the signal-to-noise ratio (see, e.g. [35]).

5. Vision of fast CARS applied to detect aflatoxin in a nanoantenna array

Use of electron beam lithography to pattern a nanoantenna array alternation with aflatoxin binding sites is within the realm of current technology. One embodiment is depicted in Figure 4 where we envision immobilizing aflatoxin antibodies on specific sites or grooves. The work of Qian *et al*. [36] in which they studied the binding of monoclonal antibodies (specific to the hepatitis B antigen) on polystyrene surfaces is a good example. The studies of Phillips and co-worker [37] demonstrating the absorption of aflatoxin B_1 on the smectite clay (hydrated sodium calcium aluminoscilate HSCAS) is another example.

Insight into potential mechanisms for the absorption of AfB_1 onto the surface of nanostructures came from the observation that stereochemical differences between some of the aflatoxin analogues resulted in a significant effect on the absorptions (even though the carbonyl functional groups were identical). AfB_1 and analogues are relatively planar compounds except for the dihydrofuran groups. Interestingly, the analogues that possess the functional group extending out of the major plane of the molecule in the opposite direction of the furan group show a significantly weaker binding. These results also suggest that the molecular mechanism for the absorption of aflatoxins onto nanostructures may favour an optimal orientation where the furan is aligned away from the surface.

In many cases it is clear AfB_1 is strongly bound (chemisorbed) to HSCAS. A potential chemical reaction that may explain these results is an electron donor acceptor (EDA) mechanism. This mechanism involves sharing electrons from the negative surface of the clay with atoms in the absorbed molecule that are partially positive [38]. The carbons compromising the dicarbonyl system in aflatoxins are partially positive (electron poor) and have also been shown to be essential to the absorption process.

An antenna array could be prepared by coating an appropriate substrate, e.g. a smooth HSCAS surface with an appropriate film which is then exposed via beam lithography to rule an array of dipole antennas. After lift off, a sandwich of alternating conducting nanoantenna/$Af\ell B_1$ binding centres is prepared as in Figure 7.

In order to support our design we performed a numerical analysis on a dipole array, a portion of which is shown in Figure 8(a). The array is excited by a 1000 nm dual polarized plane wave with the two polarizations in phase quadrature. The gold dipoles making up the array lie on an ITO layer above a glass substrate as shown in Figure 8(b). In this simulation the dipoles have a gap width of 10 nm, are 10 nm high, 10 nm wide, and have a resonant length of 43 nm, one-half a surface plasmon wavelength. Although it is possible to make the gap width between the individual dipole elements much less than 10 nm, thereby increasing enhancement, our design is based on the assumption that a large number of $Af\ell B_1$ molecules will be present in the gap, thus lowering the required enhancement level.

Our computer simulations take into account the finite metallic conductivity at optical frequencies by using a Lorentz–Drude expression [39],

$$\epsilon(\omega) = \epsilon_{\mathrm{L}}(\omega) + \epsilon_{\mathrm{D}}(\omega),$$

where

$$\epsilon_{\mathrm{L}}(\omega) = \epsilon_\infty + \sum_{n=1}^{N} \frac{f_n\omega_{\mathrm{p}}^2}{(\omega^2 - \omega_n^2) + \mathrm{i}\omega\Gamma_n}$$

is the Lorentz damped oscillator model and

$$\epsilon_{\mathrm{D}}(\omega) = \epsilon_\infty - \frac{\omega^2}{\omega^2 - \mathrm{i}\omega\Gamma_0}$$

is the Lorentz–Drude model. In the above ω_{p} is the plasma frequency, Γ is the damping factor, and ω_n is

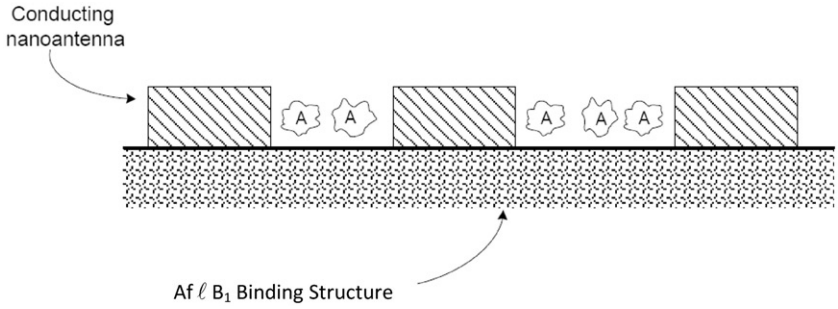

Figure 7. Lithographically prepared antenna array with grooves in which AfℓB$_1$ is preferentially bound to the clay substrate.

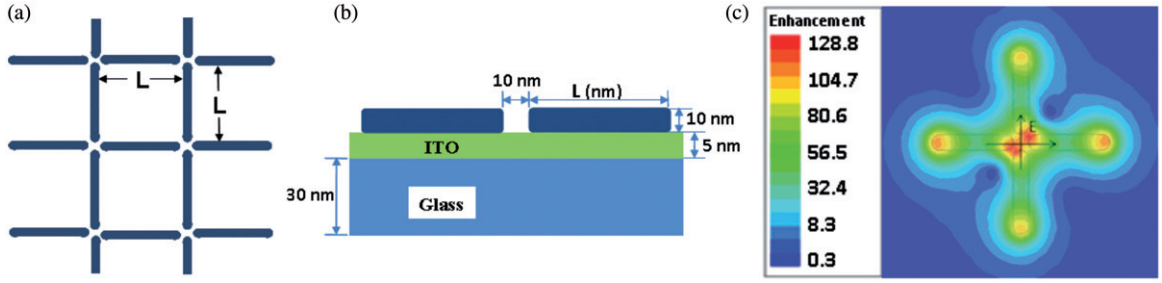

Figure 8. A cross-dipole arrangement with (a) dipole arms a resonant length $L = 43$ nm arranged in an array pattern. (b) The array elements are gold strips lying on an ITO layer above glass and are illuminated from above by a 1000 nm dual polarized plane wave (c) which achieves an enhancement of 128.8 above the dipole gap in a plane 15 nm above the ITO surface, the typical height of antibodies.

the resonant frequency. Even with a relatively wide 10 nm gap the results in Figure 8(c) of our computer simulation recorded in a plane 5 nm above the surface of the dipoles show that a large amplitude field is concentrated around the gap with an enhancement of 128.8. The observation plane which is 15 nm above the binding surface at the bottom of the gap is the typical height of antibodies. The cross-dipole arrangement will increase the chances that an incident field polarization component will align with individual AfℓB$_1$ molecules so as to produce maximum signal.

The present adaption of the FAST CARS technique to the detection of AfℓB$_1$ is based on available technology. However the present laboratory demonstration is just that, a 'laboratory demonstration'. That is the proof-of-principal experiments have been typically done with elaborate, expensive, and bulky amplified femtosecond systems. These systems allowed great flexibility in exploring the experimental parameter space and finding the optimal operation point. Once the optimal configuration is found, the next step toward real-life applications is miniaturization and cost reduction. A possible route is to use a femtosecond fibre laser. Compact-diode-pumped femtosecond fibre laser oscillators are now available at relatively low cost. Additionally, due to the pump diodes stemming from established telecommunication applications, operating costs are low and reliability is high. Feasibility of using an erbium-doped fibre mode-locked oscillator for microanalytical spectroscopy has already been demonstrated [40].

Extensions along these lines are challenging. Femtosecond fibre lasers are typically not easily tunable (even though nowadays they are available at several set wavelengths). However, a promising solution is the use of photonic crystal fibres (PCFs) that are known to allow efficient frequency conversion while preserving femtosecond pulse duration, even at low (nJ) pulse energies. In principle, these PCFs can be engineered to produce desired pulse configurations (wavelengths, shapes, delays). The problem is that the pulse energy is low. Here the nanoantenna field enhancement holds very real promise. Moreover, that is, the nanoantenna technology provides orders-of-magnitude field enhancement, essentially leading to a concentration of the laser pulse energy onto a 'hot-spot' volume which is far below the diffraction limit. This can lead to reduced pulse energy requirements and to further miniaturization of the laser system. Conceptually, the resultant system would then take

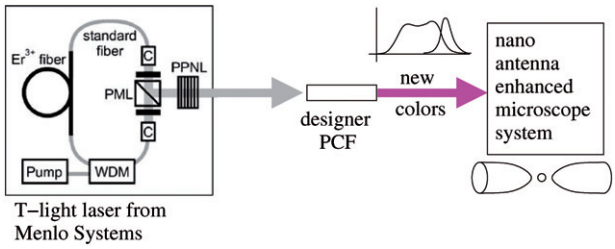

Figure 9. Spectroscopic scheme combining fiber laser, pulse shaping and nanoantenna arrays.

the form sketched in Figure 9 which combines the nonlinear spectroscopy technique of [40] and nanoantenna arrays.

Acknowledgements

The authors would like to thank V. Cholleti for carrying out the numerical calculations on the field enhancement structures presented in this paper. We acknowledge support from the National Science Foundation, the Office of Naval Research, the Army Research Office, and the Robert A. Welch Foundation (Grants No. 1261 and No. 1547).

References

[1] D.R. Herschbach, J. Chem. Phys. **84**, 838 (1986).
[2] D.R. Herschbach, J.S. Avery and O. Goscinski, editors, *Dimensional Scaling in Chemical Physics* (Kluwer Academic, Dordrecht, 1992).
[3] D.R. Herschbach, Int. J. Quantum Chem. **57**, 295 (1996).
[4] A.A. Svidzinsky, M.O. Scully and D.R. Herschbach, Phys. Rev. Lett. **95**, 080401 (2005).
[5] N. Bohr, Philos. Mag. **26**, 1 (1913).
[6] N. Bohr, Philos. Mag. **26**, 857 (1913).
[7] A.A. Svidzinsky, M.O. Scully, and D.R. Herschbach, Proc. Natl. Acad. Sci. U.S.A. **102**, 11985 (2005).
[8] *Bohr Collected Works* (North-Holland, Amsterdam, 1981), Vol. 2, p. 153.
[9] A. Sommerfeld, *Atomic Structure and Spectral Lines*, 3rd ed. (E.P. Dutton, New York, 1923), pp. 76–78.
[10] G.N. Lewis, J. Am. Chem. Soc. **38**, 762 (1916).
[11] A. Svidzindky, S. Chin, G. Chen, M. Kim, D. Ma, R. Murawski, A. Sergeev, M.O. Scully and D. Herschbach, Int. Rev. Phys. Chem. **27**, 665 (2008).
[12] M.J. Sweeney, S. White, A.D.W. Dobson, Ir. J. Agric. Food Res. **29**, 235 (2000); J.L. Richard, and K. Fleetwood, Food Saf. Mag. **Dec–Jan**, 18 (2001–2002).
[13] http://upload.wikimedia.org/wikipedia/commons/7/7f/Aflatoxin B1.svg, downloaded 19 May, 2009.
[14] C.M. Maragos, J. Toxicol. **23**, 317 (2004).
[15] D. Pestov, R.K. Murawski, G.O. Ariunbold, X. Wang, M. Zhi, A.V. Sokolov, Vl.A. Sautenkov, Yu.V. Rostovtsev, A. Dogariu, Y. Huang and M.O. Scully, Science **316**, 265 (2007).
[16] A. Dogariu, Y. Huang, Y. Avitzour, R.K. Murawski and M.O Scully, Opt. Lett. **31**, 3176 (2006).
[17] M. Marangoni, A. Gambetta, C. Manzoni, V. Kumar, R. Ramponi and G. Cerullo, Opt. Lett. **34**, 3262 (2009).
[18] R. Selm, M. Winterhalder, A. Zumbusch, G. Krauss, T. Hanke, A. Sell and A. Leitenstorfer, Opt. Lett. **35**, 3282 (2010).
[19] M.O. Scully, G.W. Kattawar, R.P. Lucht, T. Opatrn, H. Pilloff, A. Rebane, A.V. Sokolov, and M.S. Zubairy, Proc. Natl. Acad. Sci. U.S.A. **99**, 10994 (2002).
[20] M. Fleischmann, P.J. Hendra and A.J. McQuillan, Chem. Phys. Lett. **26**, 163 (1974).
[21] D.L. Jeanmaire and R.P. van Duyne, J. Electroanal. Chem. **84**, 1 (1977).
[22] M.G. Albrecht and J.A. Creighton, J. Am. Chem. Soc. **99**, 5215 (1977).
[23] For a review on surface-enhanced spectroscopy see M. Moskovits, Rev. Mod. Phys. **57**, 783 (1985); P.L. Stiles, J.A. Dieringer, N.C. Shah, and R.P. van Duyne, Annu. Rev. Anal. Chem. **1**, 601 (2008).
[24] K. Kneipp, Y. Wang, R.R. Dasari and M.S. Feld, Appl. Spectrosc. **49**, 780 (1995).
[25] K. Kneipp, Y. Wang, H. Kneipp, L.T. Perelman, I. Itzkan, R.R. Dasari and M.S. Feld, Phys. Rev. Lett. **78**, 1667 (1997).
[26] S. Nie and S.R. Emory, Science **275**, 1102 (1997).
[27] T. Vo-Dinh, Trends Anal. Chem. **17**, 557 (1998).
[28] A. Aroca, *Surface-enhanced Vibrational Spectroscopy* (Wiley, New York, 2006).
[29] A.M. Michaels, M. Nirmal and L.E. Brus, J. Am. Chem. Soc. **121**, 9932 (1999).
[30] J.A. Dieringer, R.B. Lettan, K.A. Scheidt and R.P. van Duyne, J. Am. Chem. Soc. **129**, 16249 (2007).
[31] J.P. Camden, J.A. Dieringer, Y. Wang, D.J. Masiello, L.D. Marks, G.C. Schatz and R.P. van Duyne, J. Am. Chem. Soc. **130**, 12616 (2008).
[32] C.G. Khoury and T. Vo-Dinh, J. Phys. Chem. C **112**, 18849 (2008).
[33] F.J. García-Vidal and J.B. Pendry, Phys. Rev. Lett. **77**, 1163 (1996).
[34] H. Xu, J. Aizpurua, M. Kall and P. Apell, Phys. Rev. E. **62**, 4318 (2000).
[35] E.J. Liang, A. Weippert, J.M. Funk, A. Materny and W. Kiefer, Chem. Phys. Lett. **227**, 115 (1994).
[36] W. Qian, D. Yao, F. Yu, B. Xu, R. Zhou, X. Bao and Z. Lu, Clin. Chem. **46**, 1456 (2000).
[37] P. Grant, T. Philips and J. Agric, Food Chem. **46**, 599 (1998).
[38] S.B. Haderlein, K.W. Weissmahr and R.B. Schwarzenbach, Environ. Sci. Technol. **30**, 612 (1996).
[39] W.H.P. Pernice, F.P. Payne and D.F. Gallagher, Opt. Quantum Electron. **38**, 843 (2006).
[40] B. von Vacano, J. Rehbinder, T. Buckup and M. Motzkus, Appl. Phys. B **91**, 213 (2008).